SCIENTIFIC REPORTS

OPEN

SUBJECT AREAS:
PHYSIOLOGY
BIOPHYSICS

Received
16 April 2013

Accepted
5 September 2013

Published
26 September 2013

Correspondence and requests for materials should be addressed to A.T. (atakeuti@u-fukui.ac.jp)

* Current address: Department of Integrative Physiology, Faculty of Medical Sciences, University of Fukui, 23-3, Matsuokashimoaizuki, Eiheiji-cho, Yoshida-gun, Fukui 910-1193, Japan

The mitochondrial Na^+-Ca^{2+} exchanger, NCLX, regulates automaticity of HL-1 cardiomyocytes

Ayako Takeuchi[1]*, Bongju Kim[2] & Satoshi Matsuoka[2]*

[1]Department of Physiology and Biophysics, Graduate School of Medicine, Kyoto University, Yoshida-konoe, Sakyo-ku, Kyoto 606-8501, Japan, [2]Center for Innovation in Immunoregulative Technology and Therapeutics, Graduate School of Medicine, Kyoto University, Yoshida-konoe, Sakyo-ku, Kyoto 606-8501, Japan.

Mitochondrial Ca^{2+} is known to change dynamically, regulating mitochondrial as well as cellular functions such as energy metabolism and apoptosis. The NCLX gene encodes the mitochondrial Na^+-Ca^{2+} exchanger (NCX_{mit}), a Ca^{2+} extrusion system in mitochondria. Here we report that the NCLX regulates automaticity of the HL-1 cardiomyocytes. NCLX knockdown using siRNA resulted in the marked prolongation of the cycle length of spontaneous Ca^{2+} oscillation and action potential generation. The upstrokes of action potential and Ca^{2+} transient were markedly slower, and sarcoplasmic reticulum (SR) Ca^{2+} handling were compromised in the NCLX knockdown cells. Analyses using a mathematical model of HL-1 cardiomyocytes demonstrated that blocking NCX_{mit} reduced the SR Ca^{2+} content to slow spontaneous SR Ca^{2+} leak, which is a trigger of automaticity. We propose that NCLX is a novel molecule to regulate automaticity of cardiomyocytes via modulating SR Ca^{2+} handling.

Mitochondria have long been known as an ATP producing factory as well as a Ca^{2+} store[1,2]. Mitochondrial Ca^{2+} ($Ca^{2+}{}_{mit}$), which dynamically changes upon stimulation by various ligands, plays important roles in regulating mitochondrial as well as cellular functions such as energy metabolism and apoptosis[1,3–6]. The dynamic change of cytoplasmic Ca^{2+} ($Ca^{2+}{}_i$) also depends on mitochondrial function, which in turn regulates cellular function. Impairment of mitochondrial function results in the alteration of $Ca^{2+}{}_i$ dynamics in ventricular myocytes as well as sensory neurons[7–9]. Therefore, it is essential to fully understand how $Ca^{2+}{}_{mit}$ is regulated and how it affects mitochondrial and cellular functions. Studies on molecular mechanisms of $Ca^{2+}{}_{mit}$ dynamics and their linkage to cellular functions have only just begun.

Ca^{2+} enters mitochondria mainly through a Ca^{2+} selective channel, the Ca^{2+} uniporter, driven by the large negative membrane potential[10,11], and $Ca^{2+}{}_{mit}$ is extruded by the Na^+-Ca^{2+} exchanger (NCX_{mit}; predominantly active in excitable tissues such as heart) and/or the H^+-Ca^{2+} exchanger (HCX_{mit}; preferentially active in non-excitable tissues such as liver)[1,12,13]. NCX_{mit} was first discovered by Carafoli *et al.*[14], the mechanisms and roles of which have been studied in various types of tissues including brain, adrenal cortex, parotid gland, skeletal muscle and heart[15]. Using permeabilized ventricular myocytes, we have demonstrated that Ca^{2+} extrusion by NCX_{mit} is electrogenic and depends on mitochondrial membrane potential, being facilitated by the negative membrane potential[16]. In the past few years, genes encode the mitochondrial Ca^{2+} carriers, Ca^{2+} uniporter (MCU) and NCX_{mit} (NCLX, also known as NCKX6), were discovered[11,13]. We clarified that NCLX[17], a gene responsible for NCX_{mit} in HEK293, SHSY-5Y, and CHO cells[13], functions as NCX_{mit} also in B lymphocytes and acts as Ca^{2+} provider to endoplasmic reticulum (ER)[18,19]. From extensive analyses, we elucidated that NCLX-mediated Ca^{2+} recycling between mitochondria and ER is pivotal in maintaining Ca^{2+} responses to antigen of B lymphocytes[18]. Based on the studies, we hypothesized that the NCLX-mediated Ca^{2+} communication between sarcoplasmic reticulum (SR) and mitochondria has an important role also in cardiac myocytes in which $Ca^{2+}{}_i$ repetitively changes. In fact, arrhythmia is known as a feature often associated with patients of mitochondrial diseases[20,21]. Several mitochondrial as well as nuclear genes have been reported to possess mutations in these patients[22]. However the mechanisms for causing the arrhythmia are yet to be determined, although abnormality of $Ca^{2+}{}_{mit}$ handling is assumed to be involved in[23,24].

In the present study, we investigated the roles of NCLX in cardiomyocytes using HL-1, a spontaneously beating cardiac cell line originating from mouse atrial myocytes[25]. Although HL-1 cells are spontaneously beating, they are distinct from normal cardiac pacemaker cells in the ultrastructure and action potential configurations[25].

Nevertheless, the important advantage of using HL-1 is that it can be genetically manipulated easily to modulate the function or expression of a targeted protein. By performing live cell imaging as well as electrophysiological experiments, we discovered that NCLX regulates the automaticity. Detailed mechanisms were analysed using a newly developed mathematical model of HL-1 cardiomyocytes.

Results

NCLX functions as NCX_{mit} in HL-1 cardiomyocytes and regulates Ca^{2+}_{mit}. HL-1 cardiomyocytes derived from mouse atrial cells retained the phenotype of differentiated atrial myocytes[26]; they were mitochondria- and SR- rich, and T-tubules were less developed (Fig. 1a). The close localization of SR and mitochondria suggest functional coupling between the two organelles as suggested in previous studies[27–33]. Mouse NCLX (mNCLX) labelled with TagGFP2 at its C-terminus exclusively co-localized with mitochondria-targeted fluorescence protein, TagRFP-mito (Fig. 1b, Pearson's co-localization coefficient = 0.75 ± 0.03, n = 12), indicating that NCLX expresses in mitochondria of HL-1 cells. mNCLX knockdown by the use of siRNA caused 50.7 ± 8.8% (N = 3) and 42.1 ± 11.7% (N = 3) reduction of NCLX mRNA and protein expressions, respectively (see also Fig. 1c). Figure 1d, e represents the NCX_{mit} activity in HL-1 cells. In control siRNA-transfected cells whose plasma membrane was permeabilized and superfused with 10 μM Ca^{2+}, simultaneous

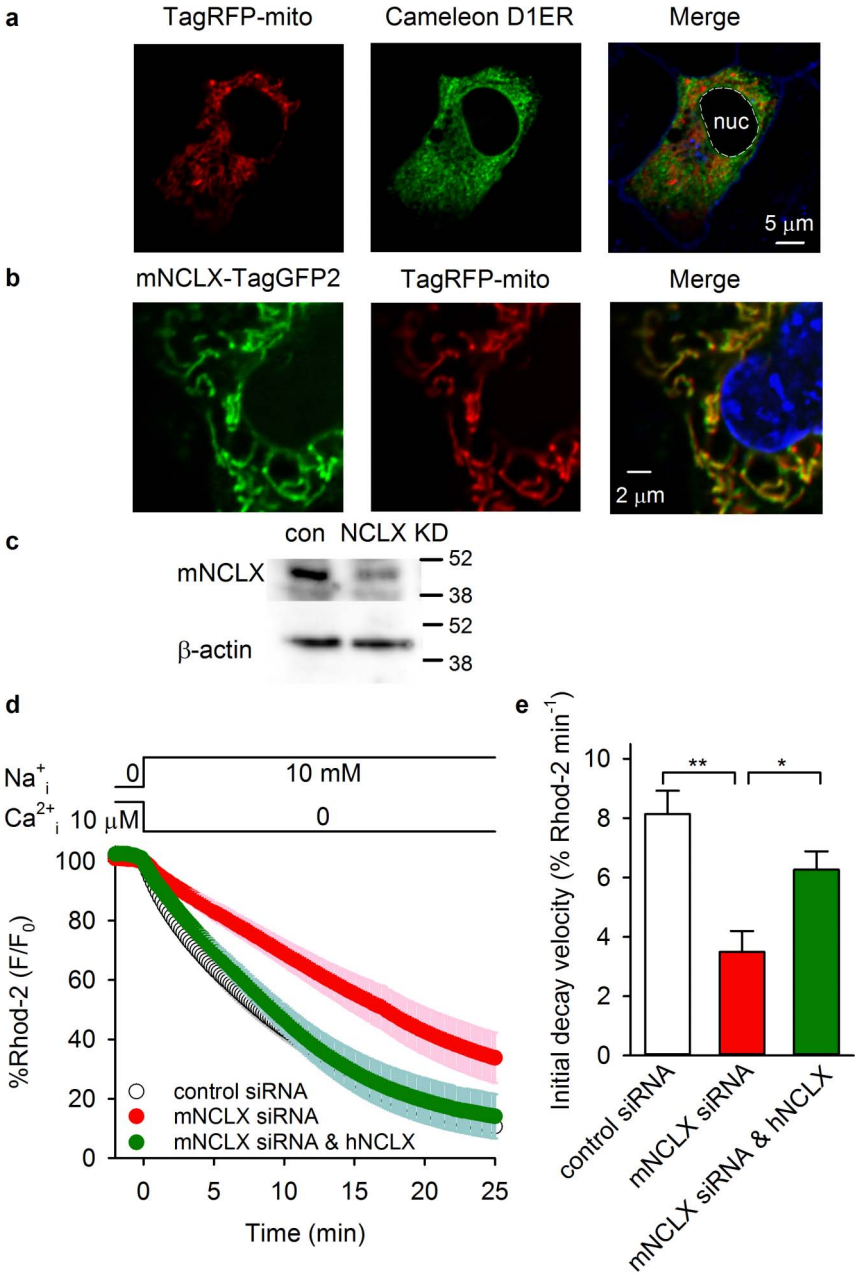

Figure 1 | NCLX is responsible for NCX_{mit} in HL-1 cardiomyocytes. (a) Mitochondria (TagRFP-mito, red) and SR (Cameleon D1ER, green) were localized close together. A merged image is shown on the right with plasma membrane stained by di-8-ANEPPS (blue). nuc: nucleus. (b) mNCLX labelled with TagGFP2 (green) and mitochondria (TagRFP-mito, red) were co-localized. The nucleus was stained by Hoechst 33342 (blue) and the merged image is shown on the right. (c) Expression of mNCLX protein was reduced in mNCLX siRNA-transfected cells. β-actin was used as a reference. con; control siRNA. NCLX KD; mNCLX siRNA. (d), (e) NCX_{mit} activity was measured in cells transfected with control siRNA (control siRNA; white), mNCLX siRNA (mNCLX siRNA; red) and mNCLX siRNA with hNCLX plasmid (mNCLX siRNA & hNCLX; green). Initial velocity of Ca^{2+}_{mit} decay was significantly decreased by knocking down NCLX but recovered by co-expressing hNCLX with mNCLX siRNA (N = 4–6). * $P < 0.05$, ** $P < 0.01$.

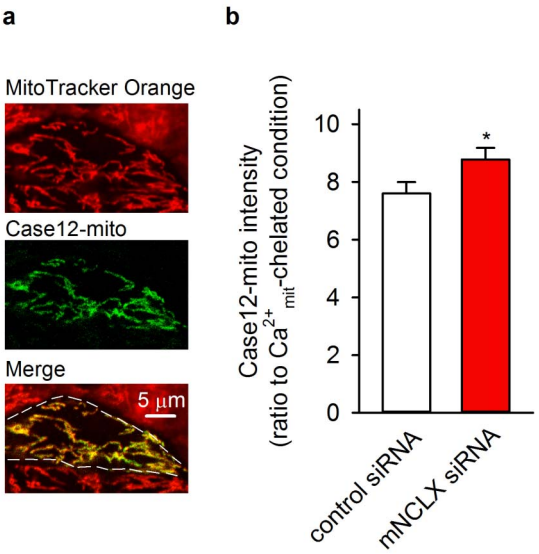

Figure 2 | NCLX knockdown increases the Ca^{2+}_{mit} in intact cells. (a) Case12-mito (green) was localized in mitochondria (MitoTracker Orange, red). A merged image is shown on the bottom. (b) Case12-mito was co-transfected with control (control siRNA; white) or mNCLX siRNA (mNCLX siRNA; red) into HL-1 cardiomyocytes. The Ca^{2+}_{mit} content, evaluated by normalizing the Case12-mito fluorescence of beating HL-1 cells to that of cells under a Ca^{2+}_{mit}-chelated condition, was markedly decreased by knocking down NCLX (N = 15–16). * $P < 0.05$ vs control siRNA.

Ca^{2+}_i removal and 10 mM Na^+_i addition induced clear fluorescence decrease of a Ca^{2+}_{mit} indicator Rhod-2, demonstrating Na^+_i-induced Ca^{2+}_{mit} extrusion (NCX_{mit} activity; white circles and column). This NCX_{mit} activity was markedly slowed by knocking down NCLX (red circles and column). Concurrent transfection of mNCLX siRNA and human NCLX (hNCLX) plasmid, whose corresponding regions are not complementary to siRNA, successfully compensated the NCX_{mit} activity (green circles and column). Note that the time course of Rhod-2 intensity increase and the peak level of Rhod-2 intensity upon 10 μM Ca^{2+} application in the absence of Na^+ was comparable between the control siRNA and mNCLX siRNA transfected cells (supplementary Fig. S1). The results suggested that the mitochondrial Ca^{2+} buffering capacity and Ca^{2+} uniporter activity were not altered by NCLX knockdown. In addition, mitochondrial membrane potential as evaluated with a ratiometric mitochondrial membrane potential indicator, JC-1, was not altered by knocking down NCLX (JC-1 intensities expressed as Red/Green ratio was 0.69 ± 0.092 and 0.68 ± 0.12 for control siRNA and mNCLX siRNA transfected cells, respectively (N = 10).

Furthermore, we measured Ca^{2+}_{mit} in beating cells by using Case12-mito, which is a Ca^{2+} sensitive fluorescence sensor targeted to mitochondria (Fig. 2a). The content of Ca^{2+}_{mit} was significantly larger in NCLX knockdown cells (Fig. 2b), indicating NCLX functions as Ca^{2+}_{mit} extrusion. Although Ca^{2+}_i spontaneously oscillated as indicated by simultaneously loaded Ca^{2+}_i indicator Rhod-3, Ca^{2+}_{mit} oscillation was hardly detected (Supplementary Fig. S2). The lack of Ca^{2+}_{mit} oscillation is probably due to the rapid beating rate of HL-1 cells (~3.5 Hz) as reported by Lu *et al.*[34].

These results demonstrated that NCLX is responsible for NCX_{mit} activity and extrudes Ca^{2+} out of mitochondria in intact HL-1 cardiomyocytes.

Automaticity of HL-1 cardiomyocytes is impaired by knocking down NCLX. Surprisingly, NCLX knockdown resulted in the prolongation of the interval between spontaneous Ca^{2+}_i transients, that is, the automaticity of HL-1 cardiomyocytes was impaired by knocking down NCLX (Fig. 3). This prolongation was rescued by a concurrent transfection of mNCLX siRNA and hNCLX. Ratiometric measurements of Ca^{2+}_i with Indo-1, which enabled us to compare the Ca^{2+}_i level among the three groups, revealed that Ca^{2+}_i levels at rest and peak, as well as the amplitude of the Ca^{2+}_i transients were not significantly different (Fig. 3b). The effect of silencing NCLX on the interval between spontaneous Ca^{2+}_i transients was also confirmed by pharmacologically inhibiting NCLX with CGP-37157 (IC_{50} = 0.36 μM[35]), an inhibitor of NCX_{mit} (Supplementary Fig. S3). Treatment of cells with up to 0.2 μM CGP-37157 did not show significant effects on the parameters of spontaneous Ca^{2+}_i transients. However, CGP-37157 markedly prolonged the cycle length and slightly but significantly decreased the resting Ca^{2+}_i level at 2 μM, and completely stopped the spontaneous Ca^{2+}_i transients at 20 μM. It should be noted that CGP-37157 also inhibits L-type Ca^{2+} channels (I_{CaL}) with IC_{50} of 0.3 μM[36]. Therefore the prolongation of the cycle length by CGP-37157 might be due to a combined inhibition of NCX_{mit} and I_{CaL}. In order to assess the individual contributions of NCX_{mit} and I_{CaL} to the increase in cycle length caused by CGP-37157, we used an I_{CaL} specific blocker, nifedipine (IC_{50} of nifedipine for I_{CaL} is ~ 0.3 μM[37]). As shown in Supplementary Fig. S4, nifedipine also prolonged the cycle length. However, it markedly decreased the resting and peak Ca^{2+}_i level and the amplitude of Ca^{2+}_i transient especially at 0.2 and 2 μM. This property was distinct from the effect of CGP-37157. The result suggests that the effect of CGP-37157 on I_{CaL} was negligible in HL-1 cells. Therefore the prolongation of cycle length caused by CGP-37157 application is likely to be resulting from NCX_{mit} blockade in HL-1 cells, which supports the findings obtained by using NCLX siRNA. On the other hand, inhibition of the mitochondrial Ca^{2+} uniporter by 5 μM Ru360 did not affect the spontaneous Ca^{2+} transient rate nor did it affect Ca^{2+}_i levels (Supplementary Fig. S5). Collectively it is strongly suggested that NCLX plays an important role in regulating the rate of the spontaneous Ca^{2+}_i transient or automaticity in HL-1 cardiomyocytes.

NCLX knockdown slows upstrokes of action potential and Ca^{2+} transient. In order to clarify the mechanisms, we examined the effect of NCLX knockdown on action potential configuration. Representative recordings and parameters for action potentials of control siRNA- or mNCLX siRNA-transfected cells are shown in Figure 4a and Table 1, respectively. Consistent with the results obtained by measuring Ca^{2+}_i transients, intervals between action potentials were significantly prolonged in mNCLX siRNA-transfected cells compared with those in control siRNA-transfected cells (Table 1). Maximum diastolic potential, peak potential, and thus amplitude of the action potential were not different between the two groups. Maximum rate of rise of the membrane potential (Vm) was also not altered. Action potential duration (APD) at 90% repolarization, APD90, was markedly prolonged by silencing NCLX, though APD30 and APD50 (30 and 50% repolarization, respectively) were not. Note that the initial upstroke of the action potential is less steep in NCLX knockdown cells (arrow in Fig. 4a) than that in control cells. In fact, pooled data of the rate of Vm change (dVm/dt) revealed that dVm/dt between −61 mV and −39 mV were significantly smaller in NCLX knockdown cells than in control cells (Fig. 4b), suggesting a decrease of inward membrane current in this Vm range. These results suggest that slowing of initial membrane depolarization in NCLX knockdown cells is related to the prolongation of cycle length.

Which factor slowed the rate of initial membrane depolarization? Considering that NCLX is a Ca^{2+} handling protein in mitochondria, it might also affect the Ca^{2+}_i dynamics and then affect the electrophysiological characteristics of the plasma membrane. In order to obtain detailed kinetic parameters of Ca^{2+}_i dynamics, spontaneous Ca^{2+}_i transients were recorded from cells loaded with Fluo-4,

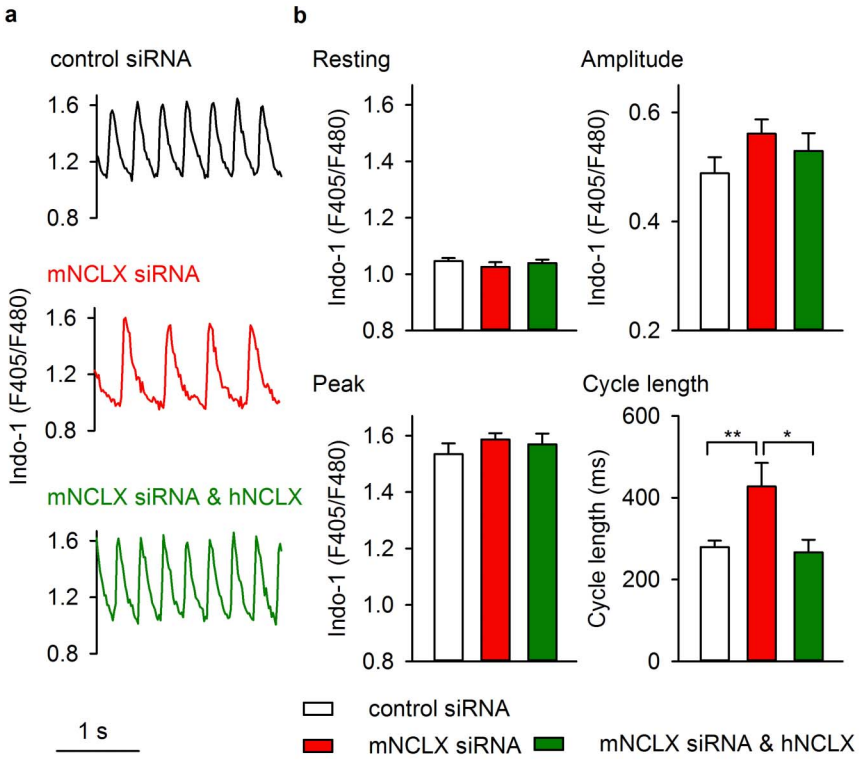

Figure 3 | The cycle length of the spontaneous Ca^{2+}_i transients is prolonged by knocking down NCLX. Spontaneous Ca^{2+}_i transients were recorded from Indo-1 loaded cells. (a) Representative recordings from cells transfected with control siRNA (control siRNA; black), mNCLX siRNA (mNCLX siRNA; red) and mNCLX siRNA with hNCLX plasmid (mNCLX siRNA & hNCLX; green). (b) Bar graphs summarizing the resting Ca^{2+}_i, peak Ca^{2+}_i and amplitude of Ca^{2+}_i transients expressed as Indo-1 fluorescence ratio (F405/F480), and cycle length of the spontaneous Ca^{2+}_i transients (N = 8). The cycle length was significantly prolonged by knocking down NCLX, but recovered by co-expressing hNCLX with mNCLX siRNA. * $P < 0.05$, ** $P < 0.01$.

AM using the line-scan mode of confocal microscopy (Fig. 4c, d). We found that the time to peak of the Ca^{2+}_i transient was considerably prolonged by knocking down NCLX. Meanwhile, the rate of Ca^{2+}_i relaxation expressed as $T_{1/2}$, and duration of the Ca^{2+}_i transient at 50% and 80% recovery, expressed as CaD50 and CaD80, were not significantly altered, though they showed tendencies to prolong. The decelerated rate of Ca^{2+}_i rise is likely to be involved in the slowed initial membrane depolarization observed in NCLX knockdown cells. It should be noted that local subsarcolemmal Ca^{2+}_i release (Ca^{2+} sparks), which was reported in a type of sinoatrial node cells[38], were detected in none of HL-1 cells recorded. We assumed that the existence of Ca^{2+} sparks is not indispensable for modulating automaticity as discussed later.

SR Ca^{2+} handling is compromised in NCLX knockdown cells. We next focused on how NCLX knockdown slowed the rate of Ca^{2+}_i rise. Recently we reported that NCLX reduction or inhibition reduced the ER Ca^{2+} uptake and ER Ca^{2+} content in B lymphocytes, thereby causing the unresponsiveness of Ca^{2+}_i upon B cell receptor stimulation[18]. Reduction of SR Ca^{2+} (Ca^{2+}_{SR}) by knocking down NCLX might also happen and affect the kinetics of Ca^{2+}_i transients in HL-1 cardiomyocytes. In order to test this hypothesis, we adopted the ratiometric fluorescence resonance energy transfer (FRET)-based SR Ca^{2+} indicator, Cameleon D1ER[39], to measure the Ca^{2+}_{SR} in intact cells. NCLX knockdown resulted in the significant decrease of Ca^{2+}_{SR} content expressed as 10 mM caffeine-responsive fraction (Fig. 5a, b). The reduced content of Ca^{2+}_{SR} might decelerate the rate of Ca^{2+}_i rise during the spontaneous Ca^{2+}_i transients in NCLX knockdown cells. The reduction of Ca^{2+}_{SR} is likely to be caused by the attenuation of SR Ca^{2+} uptake via SR Ca^{2+} pump (SERCA). As expected, the recovery of Ca^{2+}_{SR} after emptying by 10 mM caffeine was markedly decelerated in NCLX knockdown cells compared with those in control cells (Fig. 5c, d). It should be noted that expression levels of major Ca^{2+} handling proteins other than NCLX, including SERCA, were not altered by knocking down NCLX (Supplementary Fig. S6). Namely the reduction of NCLX results in the smaller supply of Ca^{2+} from mitochondria to the narrow interorganelle space, thus attenuating the Ca^{2+} uptake by SERCA to SR. In other words, functional coupling between NCLX and SERCA plays an important role in regulating Ca^{2+}_i handling of HL-1 cardiomyocytes by tuning Ca^{2+}_{SR} content.

Simulation analyses reveals that NCLX regulates automaticity by modulating SR Ca^{2+} handling. The mechanisms underlying NCLX reduction-mediated impairment of automaticity were further studied by computer simulations. We developed a computer model of HL-1 cardiomyocytes which calculates a membrane excitation and intracellular Ca^{2+} change including Ca^{2+}_{mit} fluxes, based on a human atrial cell model[40]. In short, a "mitochondria" compartment consisting of Ca^{2+} uniporter and NCX_{mit}, was incorporated in addition to existing five compartments, "extracellular space", "junctional space (JS)", "subsarcolemmmal space (SL)", "SR", and "myoplasm (cytoplasm)". The general scheme of the model is shown in Figure 6a. HL-1 cells are known to express channels related to generating automaticity, i.e. hyperpolarization-activated current (I_{ha}) and voltage-dependent T-type Ca^{2+} current (I_{CaT})[41,42] (also see Supplementary Fig. S6). We incorporated models for these currents, which can reproduce their kinetic data obtained from HL-1 cells. Likewise parameters for other components (i.e. channels) were set according to the experimental data obtained from HL-1, as far as data were available (Online Supplementary Data). This model well simulates the spontaneous action potential generation and Ca^{2+}_i transients of HL-1 cardiomyocytes (Online Supplementary Data).

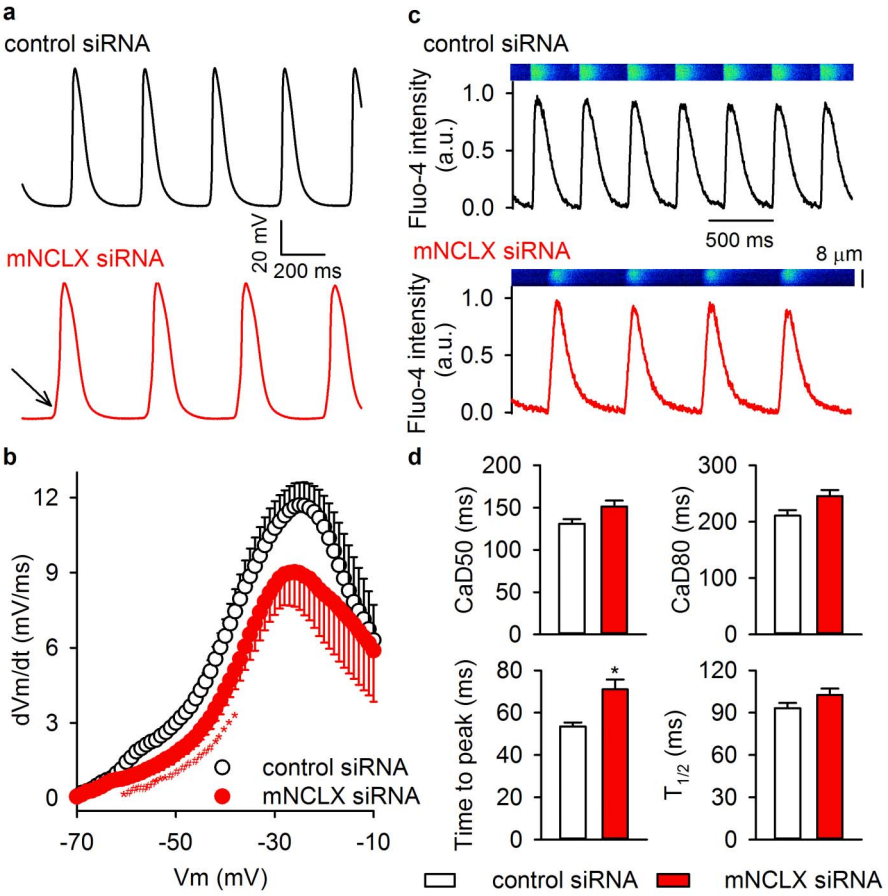

Figure 4 | NCLX knockdown alters kinetic parameters for action potential as well as Ca^{2+}_i transient. (a), (b) Action potentials were recorded from spontaneously beating HL-1 cardiomyocytes using whole-cell patch clamp method. (a) Representative recordings from cells transfected with control siRNA (black) and mNCLX siRNA (red). (b) Plot of rate of Vm change (dVm/dt) versus Vm (N = 7–8). dVm/dt was calculated with our custom software. dVm/dt around the upstroke of action potential was smaller in NCLX knockdown cells. (c), (d) Spontaneous Ca^{2+}_i transients were recorded from Fluo-4 loaded cells using a line-scan mode of confocal microscopy. (c) Representative recordings from cells transfected with control siRNA (black) and mNCLX siRNA (red). (d) Bar graphs summarize the Ca^{2+}_i transient duration (CaD) at 50% and 80% recovery (CaD50 and CaD80, respectively), time to peak Ca^{2+}_i level (time to peak), and the half time from peak Ca^{2+}_i to the full relaxation ($T_{1/2}$ of relaxation) (N = 4–5). NCLX knockdown slowed the time to peak of the Ca^{2+}_i transient. * $P < 0.05$, # $P < 0.01$ vs control siRNA.

The automaticity of HL-1 cardiomyocytes is reported to be generated by membrane channels as well as by SR Ca^{2+} handling proteins[43]. Our model well explains how SR Ca^{2+} handling proteins regulate automaticity of HL-1 cardiomyocytes. As shown in Figure 6b, where successive activations of channels and transporters are plotted as a function of Vm, the Ca^{2+}_{JS} accumulation caused by spontaneous Ca^{2+} release through ryanodine (RyR) channels triggers Ca^{2+}-induced Ca^{2+} release (CICR) again via RyR channels. Then the Ca^{2+}_{JS} accumulation activates the inward current of plasmalemmal Na^+-Ca^{2+} exchanger (I_{NCX}). This inward I_{NCX} depolarizes the Vm to activate the large inward currents in the order of voltage-dependent Na^+ current (I_{Na}), voltage-dependent I_{CaT} and I_{CaL}, to generate a large action potential.

Table 1 | Action potential parameters of HL-1 cardiomyocytes transfected with control siRNA or mNCLX siRNA

	control siRNA	mNCLX siRNA
Cycle length (ms)	328.52 ± 17.52	409.86 ± 22.83*
Maximum diastolic potential (mV)	−70.43 ± 0.43	−70.59 ± 0.39
Peak potential (mV)	9.10 ± 1.66	7.37 ± 1.42
Amplitude (mV)	79.54 ± 4.82	77.96 ± 1.13
Maximum rate of rise (mV/ms)	13.51 ± 1.19	11.23 ± 1.79
APD30 (ms)	51.31 ± 4.27	54.67 ± 1.39
APD50 (ms)	70.65 ± 5.38	76.53 ± 1.39
APD90 (ms)	143.77 ± 8.35	164.68 ± 3.89*

mean ± s.e.m. (N = 7–8), * $P < 0.05$ vs control siRNA.

The model analysis demonstrated that the smaller the amplitude factor of NCX_{mit}, the longer the cycle length becomes (Fig. 6c). It should be noted that Ca^{2+}_{SR} content decreases by reducing the amplitude factor of NCX_{mit} (Fig. 6d), well reproducing the experimental results (see Fig. 5a, b). The mechanism is demonstrated in Figure 6e–g, where simulation results using a model with 90% NCX_{mit} reduction were compared with those using a control model. Figure 6e and f showed that the decreased Ca^{2+}_{SR} causes the slower Ca^{2+} leak to the JS through RyR, thus the time of Ca^{2+}_{JS} to reach the threshold of inducing CICR becomes prolonged (Fig. 6e red line). Note that the plot of I_{NCX} vs Vm shifts rightward by reducing NCX_{mit} to 10% (inset of Fig. 6b, dashed line), meaning that the timing of I_{NCX} activation becomes delayed. The delayed activation of I_{NCX}, in other word, the smaller inward I_{NCX} at each Vm, should further contribute to the smaller dVm/dt observed in experiments (Fig. 4a, b). As a result, the cycle length increases. Upstroke of Ca^{2+}_i rise also slows because of the smaller Ca^{2+}_{SR} content with 10% NCX_{mit} (Fig. 6e, g), consistent with the experimental results (Fig. 4c, d). From the above analyses, we

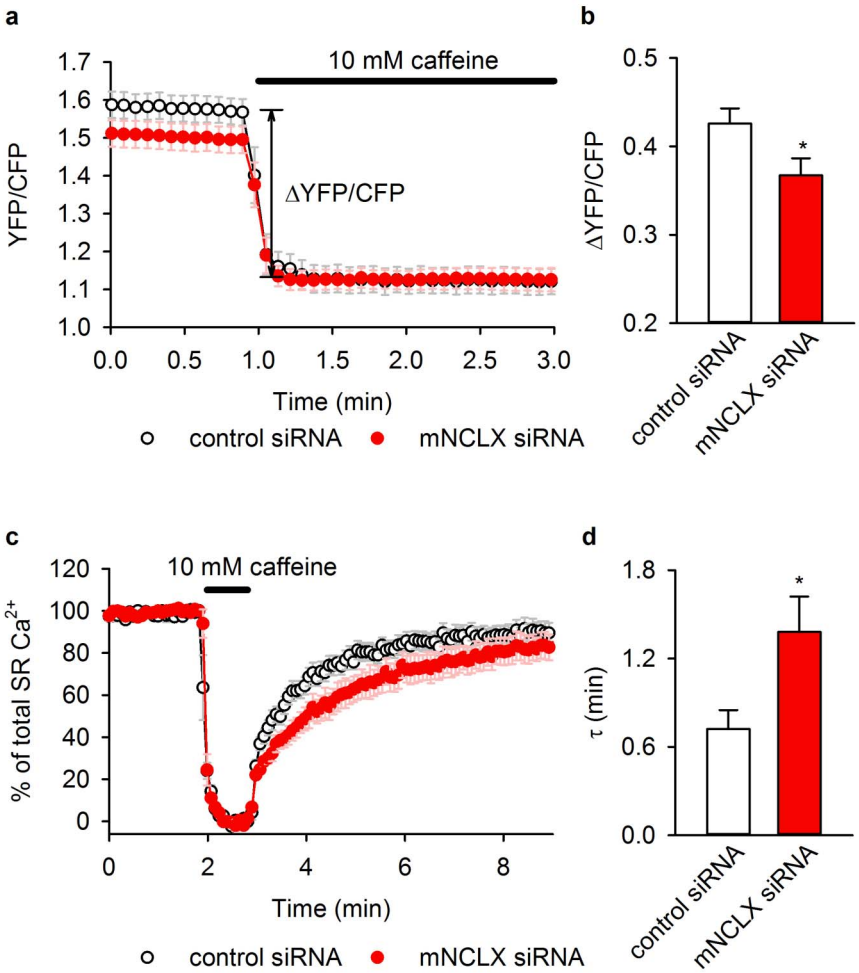

Figure 5 | SR Ca^{2+} uptake is attenuated in NCLX knockdown cells. Plasmid harbouring Cameleon D1ER, an indicator of SR Ca^{2+}, was co-transfected with control (white) or mNCLX siRNA (red) into HL-1 cardiomyoctes. (a), (b) SR Ca^{2+} content. (a)10 mM caffeine was applied to empty the Ca^{2+} in SR. $Ca^{2+}{}_{SR}$ is considered as ΔYFP/CFP. (b) Bar graph represents the summary of ΔYFP/CFP, showing that ΔYFP/CFP was significantly smaller in NCLX knockdown cells (N = 11–13). (c), (d) SR Ca^{2+} reuptake. After emptying Ca^{2+} in SR with 10 mM caffeine, recovery of YFP/CFP was measured. (d) Bar graph represents the summary of recovery time constant τ, showing that SR Ca^{2+} reuptake rate was slower in NCLX knockdown cells (N = 7–8). * $P < 0.05$ vs control siRNA.

concluded that NCX_{mit} regulates the automaticity of HL-1 cardiomyocytes through tuning the SR Ca^{2+} dynamics.

Discussion

This is the report that demonstrates the regulation of automaticity of cardiomyocytes by the mitochondrial Ca^{2+} handling protein, NCLX. In addition to finding an impairment of the automaticity by NCLX reduction, we succeeded in a mechanistic explanation of the complicated mechanism using our mathematical model (Fig. 7). That is, NCLX supplies Ca^{2+} to SR, thereby tuning the content of $Ca^{2+}{}_{SR}$, which determines the rate and extent of spontaneous SR Ca^{2+} leak through RyR channels into JS. The accumulated $Ca^{2+}{}_{JS}$ triggers the CICR via RyR channels to produce a $Ca^{2+}{}_{i}$ transient, and thus determines the activation timing of the plasma membrane I_{NCX}. The inward I_{NCX} in turn contributes to the initiation of an action potential, which occurs via subsequent activation of I_{Na}, I_{CaT} and I_{CaL}. Finally, the interval of the cycle length changes. The coupling of $Ca^{2+}{}_{i}$ homeostasis and I_{NCX} in the generation of automaticity is an well-accepted concept not only under normal but also abnormal conditions[44,45]. Our findings add a new step, SR-mitochondria Ca^{2+} communication, to the generation of automaticity. There is a large body of evidence about geometrical as well as functional communication of ER/SR and mitochondria. Ca^{2+} released from ER/SR accumulates in the interorganellar narrow space, enters mitochondria, and stimulates metabolic pathways[27–32]. Consistent with our previous report[18], the present study demonstrated that a considerable amount of Ca^{2+} is transferred from mitochondria to SR, and indicated that NCLX is one of the key players in the Ca^{2+} communication in the cardiomyocytes.

It should be emphasized that ventricular as well as atrial cells generally do not show automaticity. Therefore automaticity observed in HL-1 cardiomyocytes may be related to "abnormal" automaticity such as atrial flutter or atrial ectopic tachycardia. Whether NCLX participates in the regulation of normal automaticity in pacemaker cells is still to be studied. So far two different and controversial mechanisms have been proposed for the cardiac pacemaker activity of sinoatrial node cells; the "membrane clock" and the "Ca^{2+} clock" hypotheses. The former is a long-accepted hypothesis that the hyperpolarization-activated inward current (I_{ha}) and various other inward membrane currents contribute to the automaticity[46,47]. The latter is a relatively novel hypothesis proposing that spontaneous and cyclical Ca^{2+} release, "local subsarcolemmal Ca^{2+} releases", from the SR is the primary mechanism driving the rate, with membrane channels having at best a minor modulatory role[48]. Recently, Yaniv *et al.*, whose group proposed the "Ca^{2+} clock" hypothesis, reported data supporting our finding of NCLX-mediated regulation of

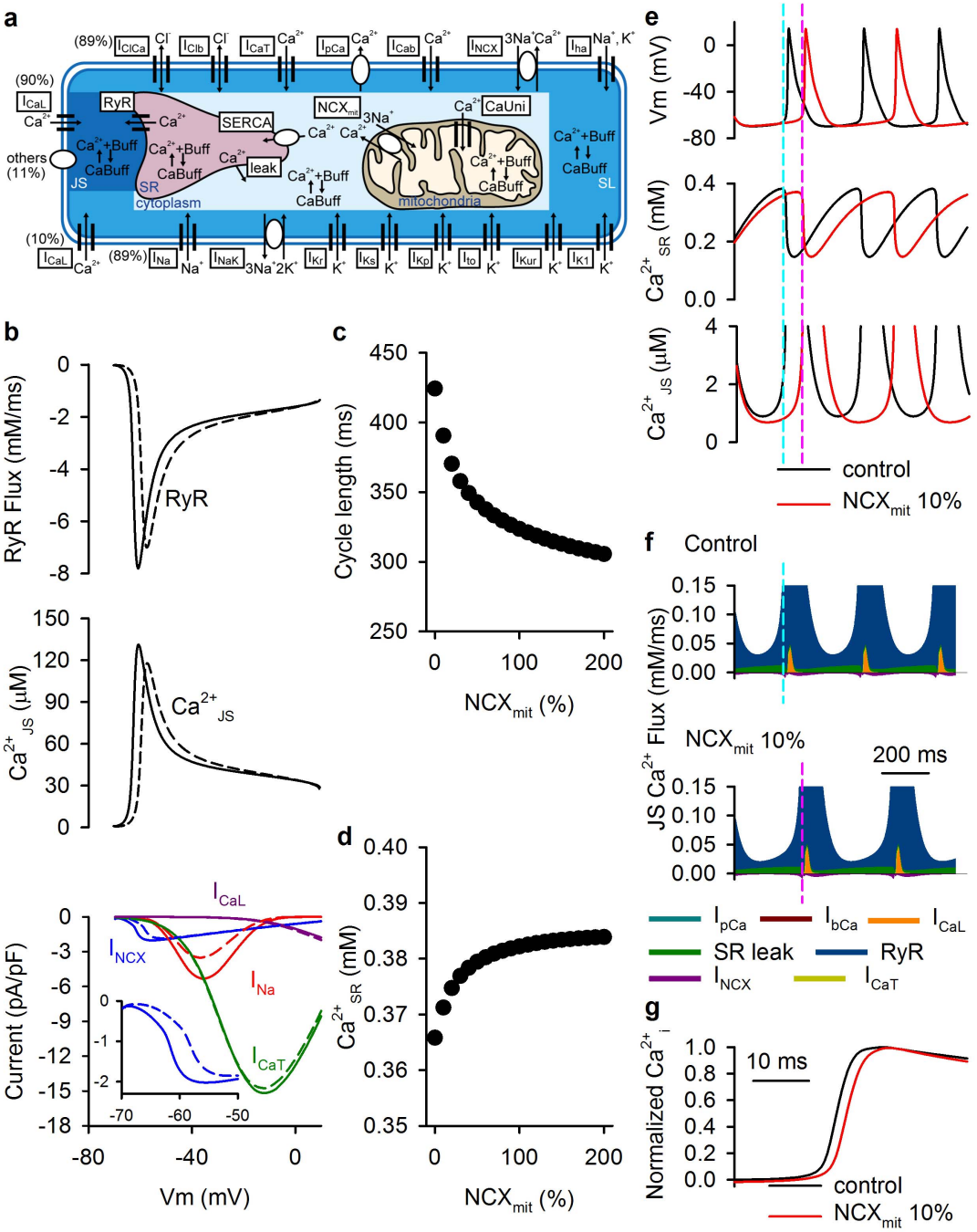

Figure 6 | NCX_{mit} reduction impairs SR Ca^{2+} handling and automaticity in HL-1 cell model. (a) Model scheme. Distributions of membrane channels and transporters in JS and SL spaces are indicated in parenthesis. (b) The relationships between RyR flux, Ca^{2+}_{JS} and various currents through transporter/channels versus Vm showed that the automaticity of HL-1 cell model is driven by spontaneous Ca^{2+} release from SR. Solid and dashed lines represent simulated data using control and 10% NCX_{mit} model, respectively. Inset shows the magnified I_{NCX} vs Vm, focusing on the initial membrane depolarization. (c), (d) The smaller the amplitude factors of NCX_{mit}, the longer the cycle length of spontaneous action potential generation (c) and the smaller the Ca^{2+}_{SR} (d) became. The model was calculated for 30 s after changing the amplitude factor of NCX_{mit}. (e–g) Effects of reducing the amplitude factor of NCX_{mit} to 10%. (e) Black and red lines represent Vm, Ca^{2+}_{SR} and Ca^{2+}_{JS} from control and 10% NCX_{mit} model, respectively. Both traces were adjusted to the timing of maximum diastolic potential. Model with 10% NCX_{mit} showed smaller Ca^{2+}_{SR} and slower Ca^{2+}_{JS} increase. (f) Contribution of components responsible for the Ca^{2+} fluxes into JS. For clarity, the timings of action potential upstrokes were indicated as dashed lines. Flux through RyR was slower in the model with 10% NCX_{mit}. (g) Initial phase of the Ca^{2+}_{i} transient. Black and red lines represent simulated data using control and 10% NCX_{mit} model, respectively. The upstroke of Ca^{2+}_{i} was decelerated in the model with 10% NCX_{mit}.

automaticity[49]. CGP-37157 prolonged the spontaneous beating rate and decreased Ca^{2+}_{SR} in rabbit sinoatrial node cells. Although the nonspecific effect of the drug on I_{CaL} cannot be denied[36], and the distinct mechanisms for generating automaticity between HL-1 cells and sinoatrial node cells should be taken into account, our current study in combination with their data suggest that NCLX tunes the automaticity of "Ca^{2+} clock"-driven sinoatrial node cells.

In regulating automaticity of HL-1 cardiomyocytes, Yang and Murray[43] reported that both "membrane clock" and "Ca^{2+} clock" mechanisms are operative, by extensively investigating the effects of

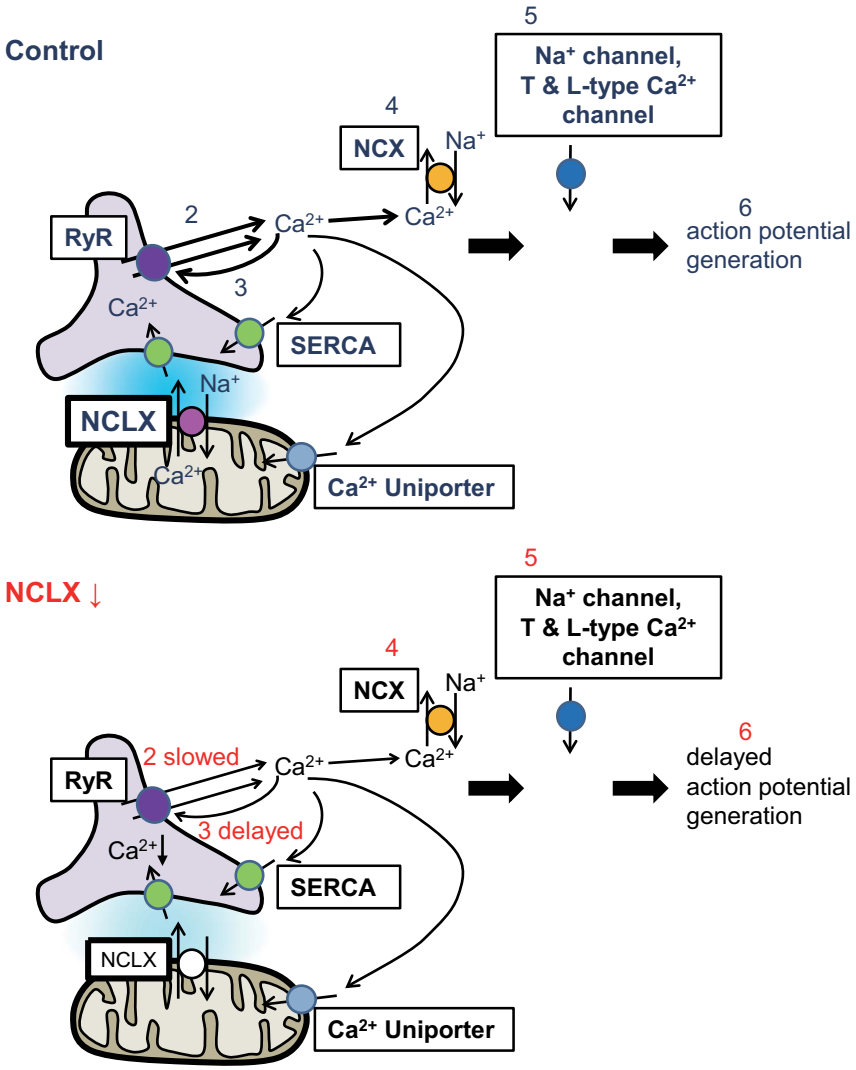

Figure 7 | Hypothetical mechanism for NCLX knockdown-mediated alteration of the automaticity. In control cardiomyocytes, NCLX supplies sufficient Ca^{2+} to SR (1). Then spontaneous Ca^{2+} leak from SR accumulates in JS (2), which at a certain point triggers the CICR via RyR channel (3). The increase of $Ca^{2+}{}_{JS}$ activates the inward current of I_{NCX} (4), which generates the initial membrane depolarization. The membrane depolarization successively activates the I_{Na}, I_{CaT} and I_{CaL} (5), resulting in the large membrane depolarization (6). In case of NCLX knockdown cells, $Ca^{2+}{}_{SR}$ content is smaller because of the smaller Ca^{2+} supply from mitochondria to SR (1). Then the spontaneous Ca^{2+} leak from SR becomes slowed due to the smaller $Ca^{2+}{}_{SR}$ (2), which results in the delay of CICR (3). Thus the activation of I_{NCX} is delayed (4), which nonetheless generates the initial membrane depolarization of the action potential. The initial membrane depolarization activates the I_{Na}, I_{CaT} and I_{CaL}, all of which are intact, resulting in the usual large action potential (5). Therefore, the delayed action potential generation (6) is due to the slowed spontaneous Ca^{2+} leak from SR.

various blockers for carriers. Our study supported their conclusion. Blocking I_{ha} by 90% in our model resulted in the marked prolongation of cycle length by ~ 80% (data not shown) and blocking SERCA prolonged the cycle length both experimentally and theoretically (Supplementary Figs. S7, S8). However, we found that "local subsarcolemmal Ca^{2+} releases (Ca^{2+} sparks)" are not indispensable for triggering automaticity and that it is the "spontaneous Ca^{2+} leak from SR" that determines the rhythm. As shown in Fig. 4c, HL-1 cells do not show any "local subsarcolemmal Ca^{2+} releases". Nevertheless, our experimental as well as theoretical analyses clarified that perturbation of SR Ca^{2+} uptake via NCLX inhibition changed the pacemaker activity of HL-1 cells. That is, regardless of the existence of "local subsarcolemmal Ca^{2+} releases", it is the "spontaneous Ca^{2+} leak from SR" which plays a major role in making rhythm of HL-1 cells. Ca^{2+} sparks are caused by spontaneous Ca^{2+} leak from SR in restricted regions of a cell. However it is hard to consider that sporadic appearance of Ca^{2+} sparks triggers the synchronized action potential in whole cell. In fact, not all beating sinoatrial node cells had detectable Ca^{2+} sparks (only 14 of 53 cells)[38]. Interestingly, Neco *et al.*[50] reported that sinoatrial node cells isolated from ryanodine receptor 2 mutant mice (RyR^{R4496C}) has slower pacemaker activity than those from wild type mice, although they had increased frequency of Ca^{2+} sparks. They also found that SR Ca^{2+} content was significantly smaller in RyR^{R4496C} sinoatrial node cells. Their results support our finding that the "spontaneous Ca^{2+} leak from SR" determined by SR Ca^{2+} content, not necessarily the "local subsarcolemmal Ca^{2+} releases", contributes to making rhythm.

SR Ca^{2+} reuptake by SERCA was significantly decreased with reduced expression of NCLX (Fig. 5c, d). One might speculate that NCLX reduction/inhibition-mediated cycle length prolongation is attributable to SERCA inhibition. In fact, SERCA reduction resulted in the prolongation of cycle length in the experiment (Supplementary Fig. S7) as well as in the model simulation (Supplementary Fig. S8). However, SERCA inhibition increased and decreased the resting and peak $Ca^{2+}{}_i$ levels, respectively, and thus significantly decreased the amplitude of the $Ca^{2+}{}_i$ transients. These phenotypes are distinct from

those obtained by applying CGP-37157 as well as by silencing NCLX using siRNA where amplitudes of $Ca^{2+}{}_i$ transients were not affected (Fig. 3, Supplementary Fig. S3).

Interestingly, no significant change of the rhythm was observed by blocking mitochondrial Ca^{2+} uniporter using Ru360, although there was a tendency to be accelerated (Supplementary Fig. S5). It might be possible that the ability of HL-1 cells to make the rhythm is at the maximum with control expression level of mitochondrial Ca^{2+} uniporter and NCX_{mit}. Our theoretical analysis showed that increase of the NCX_{mit} amplitude from 100% to 200% only slightly decreases the cycle length (~6%; Figure 6c). Another possibility is the existence of a Ca^{2+} uptake carrier different from Ca^{2+} uniporter. We confirmed by RT-PCR that Letm1, a H^+-Ca^{2+}exchanger[51], is expressed in HL-1 cells (unpublished data). Although the direction and the stoichiometry of the Ca^{2+} transport via Letm1 is still controversial[52], it might be possible that Letm1 functions to uptake Ca^{2+} into mitochondria together with mitochondrial Ca^{2+} uniporter. Although it is very interesting to examine, this is out of the scope of our present study.

$Ca^{2+}{}_i$ dynamics is known to have critical roles in making rhythmicity of tissues other than heart. For example, the initiation of pacemaker activity in the interstitial Cajal cell, which is a pacemaker cell in the gastrointestinal tract and fallopian tubes, is caused by release of ER/SR Ca^{2+} through inositol 1,4,5-trisphosphate receptor and/or RyR channel[53,54]. In addition, recent findings suggest that Ca^{2+} release from ER via RyR channels are involved in the firing of neurons[55,56]. NCLX might also supply Ca^{2+} to ER/SR of these cells, thus contributing to making rhythmicity.

Growing evidence indicates that mitochondria play roles in the genesis of arrhythmia[24,57]. In particular, factors involved in energy metabolism as well as oxidative stress have been considered as the causes of arrhythmia in mitochondrial disease[20–22]. However, neither cellular ATP nor mitochondrial reactive oxygen species were altered by knocking down NCLX in HL-1 cardiomyocytes (Supplementary Fig. S9). We propose here a new hypothesis that NCLX is one of the factors involved in the progression of arrhythmia in mitochondrial diseases. Right now, information as to NCLX mutation(s) in patients with mitochondrial diseases is lacking. Comprehensive genetic analysis will clarify whether NCLX is involved in mitochondrial diseases.

Methods

Cell culture and transfection. The mouse atrial cell line, HL-1 was a kind gift from Dr. Claycomb[25] and maintained according to the instructions.

mNCLX cDNA[18] was inserted into the pTagGFP2-N vector (Evrogen). hNCLX cDNA was purchased from Toyobo Japan. Control siRNA and mNCLX siRNA was purchased from Santa Cruz Biotechnology, Inc., and Sigma-Aldrich, respectively. A FRET-based SR Ca^{2+} indicator Cameleon D1ER/pcDNA3 was a kind gift from Dr. Tsien[39].

The day before the transfection, cells were plated onto glass bottom dishes or coverslips. For the NCLX knockdown experiments, siRNA transfection was performed using Lipofectamine™ RNAiMAX reagent (Life Technologies). Concentrations used for the transfection were, 24 nM control or mNCLX siRNA and 24 nM mNCLX siRNA + 1 μg/ml hNCLX/pME18SFL3. For the measurement of $Ca^{2+}{}_{SR}$ or $Ca^{2+}{}_{mit}$, 0.3 μg/ml Cameleon D1ER/pcDNA3 or pCase12-mito (Evrogen) was added besides control or mNCLX siRNA. For assessing mitochondrial and SR localization, 0.5 μg/ml pTagRFP-mito (Evrogen) and 0.5 μg/ml Cameleon D1ER/pcDNA3 were co-transfected using Lipofectamine™ LTX with PLUS™ reagent (Life Technologies). For assessing intracellular localization of mNCLX, 0.5 μg/ml mNCLX/pTagGFP2-N and 0.5 μg/ml pTagRFP-mito were co-transfected. Experiments were performed 48–72 hr after the transfection using sheet-like multicellular preparations. Although every cell exhibited spontaneous and synchronized beating in the majority of the preparations, a small fraction of the preparations (<10%) did not show spontaneous beating. We excluded these from the recordings.

Cellular localization of mitochondria, SR and GFP-labelled mNCLX. For assessing cellular localization of SR and mitochondria, cells co-transfected with Cameleon D1ER/pcDNA3 and pTagRFP-mito were stained with a membrane voltage sensitive dye, di-8-ANEPPS (2 μM; Life Technologies), to visualize the boundary between cells. Images were acquired using a laser scanning confocal microscope (LSM710, Carl Zeiss) with a x63 oil objective lens. Cameleon D1ER, TagRFP, and di-8-ANEPPS images were obtained with excitation at 488, 561, and 458 nm, and emission at 493–534, 563–602 and 639–758 nm, respectively.

For assessing cellular localization of NCLX, cells co-transfected with mNCLX/pTagGFP2-N and pTagRFP-mito were stained with Hoechst 33342 (200 ng/ml; Dojindo, Japan). Images were acquired using the LSM710 with a x63 oil objective lens. TagGFP2, TagRFP and Hoechst 33342 images were obtained with excitation at 488, 561, and 405 nm, and emission at 495–592, 591–759 and 410–507 nm, respectively. Co-localization of mNCLX and mitochondria was quantified by the Pearson's co-localization coefficient[58] using a plugin (JACoP) for ImageJ. The offset of each image was set automatically to avoid arbitrary judgment. Deconvolution was performed for all presented confocal images using Autoquant X2.2 (Media Cybernetics Inc.).

Analysis of expression level of NCLX. Total RNA was isolated from three different batches of control- or mNCLX siRNA-transfected cells with RNeasy Plus Mini kit (QIAGEN GmbH), then was reverse-transcribed using Transcriptor First Strand cDNA Synthesis Kit (Roche Diagnostics). Real-time PCR was performed with the SYBR green dye technique on a Light Cycler 480 (Roche Diagnostics). Reaction conditions were 95°C for 10 min, followed by 45 cycles of 95, 55 and 72°C for 10, 20 and 10 sec, respectively. Specific primers used were 5′- TCGCTGTGACTTTGTCAGGA-3′ (sense; position 338–357) and 5′-AAGCAGCCAGAAAACGTAGAGG-3′ (antisense; position 473–452) for mNCLX (NM_133221) and 5′-TGTGTCCGTCGTGGATCTGA-3′ (sense; position 761–780) and 5′- CCTGCTTCACCACCTTCTTGA-3′ (antisense; position 837–817) for glyceraldehyde-3-phosphate dehydrogenase (GAPDH, NM_008084). Expression level of mNCLX mRNA was presented as a ratio to GAPDH.

Three different batches of cells transfected with control or mNCLX siRNA were lysed with M-PER Mammalian Protein Extraction Reagent (Thermo) and were resolved by SDS-PAGE. NCLX antibody was a kind gift from Dr. Sekler[13]. The gels were transferred to PVDF membranes, blocked for 1 hr with Blocking One (Nacalai Tesque, Japan), followed by incubation with 500 × (for mNCLX) or 2,000 × (for β-actin) diluted primary antibody for 1 hr. Then the membranes were incubated with 10,000 × diluted HRP-linked donkey anti-rabbit IgG (for mNCLX; GE Healthcare) or 2,000 × diluted HRP-linked anti-mouse IgM (for β-actin; Calbiochem) for 1 hr. The image was developed with ECL Plus Western Blotting Detection Reagents (GE Healthcare) and acquired by LAS-4000 mini (Fujifilm). The intensities of the bands were quantified using ImageJ. Expression level of NCLX protein was presented as a ratio to β-actin.

Measurement of NCX_{mit} activity. $Ca^{2+}{}_{mit}$ was measured as described previously with slight modifications[16,18,19]. After incubation with 5 μM Rhod-2, AM (Life Technologies), the cells on a coverslip were transferred to a perfusion chamber on a fluorescence microscope with a perfect focus system (ECLIPSE TE2000, Nikon). Images were recorded using an EM-CCD camera (ImagEM, Hamamatsu Photonics) and analysed with AQUACOSMOS software (Hamamatsu Photonics). The plasma membrane was permeabilized by perfusing with a Ca^{2+}-free cytosol-like medium (CLM_{mit}) containing 30 μM β-escin for 60 sec. Then mitochondria were loaded with Ca^{2+} in the CLM_{mit} containing free 10 μM Ca^{2+} and no Na^+, and $Na^+{}_i$-dependent $Ca^{2+}{}_{mit}$ decrease was initiated by removal of $Ca^{2+}{}_i$ and addition of 10 mM $Na^+{}_i$. In the preliminary experiments, we measured the mitochondrial membrane potential with TMRE during 10 min application of 10 μM Ca^{2+}. If the mitochondrial transition pore opens, mitochondrial membrane potential should markedly depolarize. The TMRE fluorescence changed only by 12.1 ± 2.2% (N = 4), suggesting a slight membrane depolarization. Therefore mitochondrial transition pore hardly opened under our experimental condition. Rhod-2 images were obtained with 535 ± 25 nm excitation and 610 ± 37 nm emission at ~ 30°C. The initial velocity was measured by fitting a linear function to data at initial 3 min. The CLM_{mit} contained (in mM) 118 KCl, 10 EGTA, 10 HEPES, 3 K_2ATP, 2 K pyruvate, 1 K_2HPO_4, 2 succinate, 0.1 K-ADP, 2 malate, and 2 K glutamate (pH 7.2 with KOH). Calculated free Mg^{2+} and Ca^{2+} concentrations[59] were 1 mM and 10 μM, respectively. The CLM_{mit} containing 10 mM Na^+ was prepared by replacing KCl with equimolar NaCl.

Measurement of $Ca^{2+}{}_{mit}$. Cells co-transfected with control or mNCLX siRNA and pCase12-mito were placed on a fluorescence microscope (ECLIPSE TE2000). Images were recorded using an EM-CCD camera (ImagEM). 5 mM EGTA, 25 μM BAPTA, AM (Dojindo) and 1 μM carbonyl cyanide 4-(trifluoromethoxy) phenylhydrazone (FCCP; an uncoupler of oxidative phosphorylation in mitochondria) in Tyrode's solution were applied for 15 min to minimize $Ca^{2+}{}_{mit}$. After background subtraction, the ratio of Case12-mito intensity before : after 15 min application of these drugs was considered as $Ca^{2+}{}_{mit}$ content. The experiments were performed at ~ 30°C. Tyrode's solution contained (in mM) 140 NaCl, 5.4 KCl, 0.33 NaH_2PO_4, 0.5 $MgCl_2$, 1.8 $CaCl_2$, 5.5 glucose and 5 HEPES (pH 7.4 with NaOH).

Measurement of spontaneous $Ca^{2+}{}_i$ transients. Cells were loaded with 10 μM Indo-1, AM (Life Technologies) and the spontaneous $Ca^{2+}{}_i$ transients were measured at an interval of 15.6 ms in Tyrode's solution at ~ 37°C as in our previous study[60].

Line-scan imaging (1.4 ms/line) of Ca^{2+} transients were obtained at ~ 30°C using a laser scanning confocal microscope (FV500, Olympus). The cells were loaded with 2.5 μM Fluo-4, AM (Life Technologies). The scanning laser line was placed approximately equidistant from the outer edge of the cell and the nucleus, to ensure the nuclear area was not included in the scan line.

Electrophysiological recordings. Action potentials were recorded at 40 kHz from the cell layer by the whole-cell patch-clamp technique using an Axopatch 200B amplifier, Digidata 1440A interface and pCLAMP 10 software (Molecular Devices,

Inc.) at ~ 30°C. The Tyrode's solution was used for bathing solution. The pipette solution contained (in mM) 135 KCl, 5 Na_2 creatine phosphate, 5 MgATP, and 10 HEPES (pH 7.2 with KOH). Membrane potentials were corrected by a measured liquid junction potential of −6 mV.

Measurement of Ca^{2+}_{SR}. Cells co-transfected with control or mNCLX siRNA and Cameleon D1ER were placed on a fluorescence microscope (ECLIPSE TE2000). Fluorescence image pairs of single cells at 480 ± 30 (CFP) and 535 ± 40 nm (YFP), which were excited at 435 ± 10 nm and then separated with the W-View system (Hamamatsu Photonics), were recorded with a cooled CCD digital camera (ORCA-ER, Hamamatsu Photonics). The ratios of images of YFP to CFP were calculated after the subtraction of background fluorescence. 10 mM caffeine in Tyrode's solution was applied to empty Ca^{2+} in the SR. Therefore the difference between fluorescence ratio (ΔYFP/CFP) before and after the caffeine application was considered as $Ca^{2+}{}_{SR}$ content. SR Ca^{2+} reuptake was recorded every 5 s after washing out the caffeine, which had been applied for 1 min. In order to minimize the effect of beating rate on the YFP/CFP recovery, the beating was stopped by 2 μM nicardipine hydrochloride, an inhibitor of voltage-dependent Ca^{2+} channels. The recovery was fitted by a single-exponential equation and time constant (τ) was calculated using SigmaPlot 12 (Systat Software Inc.). The experiments were performed at ~ 30°C.

Statistical analysis. All data are presented as mean ± s.e.m. of independent experiments or independent recordings. The number of independent experiments and that of recordings (number of cells or images) from each experiment are presented as N and n, respectively. In the measurements of cell responses under the microscope, the responses from n individual recordings in each dish were averaged for each experiment N. Then the statistical evaluation was performed on these averaged responses from N independent experiments. Statistical analyses were performed by one-way ANOVA multiple comparisons (SigmaPlot 12). Multiple and two-group comparisons were performed according to the Student–Newman–Keuls method and paired or unpaired two-tailed Student's t test, respectively. $P < 0.05$ was considered significant.

A computer simulation. A mathematical model of HL-1 cells was constructed with a Java-based simulation platform, simBio[61], in a manner similar to our previous models[62–64] and its details are described in Online Supplementary Data.

1. Celsi, F. *et al.* Mitochondria, calcium and cell death: a deadly triad in neurodegeneration. *Biochim. Biophys. Acta.* **1787**, 335–344 (2009).
2. Murgia, M., Giorgi, C., Pinton, P. & Rizzuto, R. Controlling metabolism and cell death: at the heart of mitochondrial calcium signalling. *J. Mol. Cell Cardiol.* **46**, 781–788 (2009).
3. McCormack, J. G., Halestrap, A. P. & Denton, R. M. Role of calcium ions in regulation of mammalian intramitochondrial metabolism. *Physiol. Rev.* **70**, 391–425 (1990).
4. Jo, H., Noma, A. & Matsuoka, S. Calcium-mediated coupling between mitochondrial substrate dehydrogenation and cardiac workload in single guinea-pig ventricular myocytes. *J. Mol. Cell Cardiol.* **40**, 394–404 (2006).
5. Satrústegui, J., Pardo, B. & Del Arco, A. Mitochondrial transporters as novel targets for intracellular calcium signaling. *Physiol. Rev.* **87**, 29–67 (2007).
6. Glancy, B. & Balaban, R. S. Role of mitochondrial Ca^{2+} in the regulation of cellular energetics. *Biochemistry* **51**, 2959–2973 (2012).
7. Duchen, M. R., Valdeolmillos, M., O'Neill, S. C. & Eisner, D. Effects of metabolic blockade on the regulation of intracellular calcium in dissociated mouse sensory neurones. *J. Physiol.* **24**, 411–426 (1990).
8. Bers, D. M., Bassani, J. W. & Bassani, R. A. Competition and redistribution among calcium transport systems in rabbit cardiac myocytes. *Cardiovasc. Res.* **27**, 1772–1777 (1993).
9. Maack, C. *et al.* Elevated cytosolic Na^+ decreases mitochondrial Ca^{2+} uptake during excitation-contraction coupling and impairs energetic adaptation in cardiac myocytes. *Circ. Res.* **99**, 172–182 (2006).
10. Kirichok, Y., Krapivinsky, G. & Clapham, D. E. The mitochondrial calcium uniporter is a highly selective ion channel. *Nature* **427**, 360–364 (2004).
11. Baughman, J. M. *et al.* Integrative genomics identifies MCU as an essential component of the mitochondrial calcium uniporter. *Nature* **476**, 341–345 (2011).
12. Castaldo, P. *et al.* Role of the mitochondrial sodium/calcium exchanger in neuronal physiology and in the pathogenesis of neurological diseases. *Prog. Neurobiol.* **87**, 58–79 (2009).
13. Palty, R. *et al.* NCLX is an essential component of mitochondrial Na^+/Ca^{2+} exchange. *Proc. Natl. Acad. Sci. USA* **107**, 436–441 (2010).
14. Carafoli, E., Tiozzo, R., Lugli, G., Crovetti, F. & Kratzing, C. The release of calcium from heart mitochondria by sodium. *J. Mol. Cell Cardiol.* **6**, 361–371 (1974).
15. Carafoli, E. The fateful encounter of mitochondria with calcium: how did it happen? *Biochim. Biophys. Acta.* **1797**, 595–606 (2010).
16. Kim, B. & Matsuoka, S. Cytoplasmic Na^+-dependent modulation of mitochondrial Ca^{2+} via electrogenic mitochondrial Na^+-Ca^{2+} exchange. *J. Physiol.* **586**, 1683–1697 (2008).
17. Cai, X. & Lytton, J. Molecular cloning of a sixth member of the K^+-dependent Na^+/Ca^{2+} exchanger gene family, NCKX6. *J. Biol. Chem.* **279**, 5867–5876 (2004).
18. Kim, B., Takeuchi, A., Koga, O., Hikida, M. & Matsuoka, S. Pivotal role of mitochondrial Na^+-Ca^{2+} exchange in antigen receptor mediated Ca^{2+} signalling in DT40 and A20 B lymphocytes. *J. Physiol.* **590**, 459–474 (2012).
19. Kim, B., Takeuchi, A., Koga, O., Hikida, M. & Matsuoka, S. Mitochondria Na^+-Ca^{2+} exchange in cardiomyocytes and lymphocytes. *Adv. Exp. Med. Biol.* **961**, 193–201 (2013).
20. Finsterer, J. Histiocytoid cardiomyopathy: a mitochondrial disorder. *Clin. Cardiol.* **31**, 225–227 (2008).
21. Khatami, M. *et al.* Accumulation of mitochondrial genome variations in Persian LQTS patients: a possible risk factor? *Cardiovasc. Pathol.* **19**, e21–27 (2010).
22. Koopman, W. J., Willems, P. H. & Smeitink, J. A. Monogenic mitochondrial disorders. *N. Engl. J. Med.* **366**, 1132–1141 (2012).
23. Kawahara, K., Takase, M. & Yamauchi, Y. Ruthenium red-induced transition from ventricular fibrillation to tachycardia in isolated rat hearts: possible involvement of changes in mitochondrial calcium uptake. *Cardiovasc. Pathol.* **12**, 311–321 (2003).
24. Florea, S. M. & Blatter, L. A. The role of mitochondria for the regulation of cardiac alternans. *Front. Physiol.* **1**, 141 (2010).
25. Claycomb, W. C. *et al.* HL-1 cells: a cardiac muscle cell line that contracts and retains phenotypic characteristics of the adult cardiomyocyte. *Proc. Natl. Acad. Sci. USA* **95**, 2979–2984 (1998).
26. White, S. M., Constantin, P. E. & Claycomb, W. C. Cardiac physiology at the cellular level: use of cultured HL-1 cardiomyocytes for studies of cardiac muscle cell structure and function. *Am. J. Physiol. Heart Circ. Physiol.* **286**, H823–H829 (2004).
27. Mackenzie, L., Roderick, H. L., Berridge, M. J., Conway, S. J. & Bootman, M. D. The spatial pattern of atrial cardiomyocyte calcium signalling modulates contraction. *J. Cell Sci.* **117**, 6327–6337 (2004).
28. Seguchi, H. *et al.* Propagation of Ca^{2+} release in cardiac myocytes: role of mitochondria. *Cell Calcium* **38**, 1–9 (2005).
29. Csordás, G. & Hajnóczky, G. SR/ER-mitochondrial local communication: calcium and ROS. *Biochim. Biophys. Acta.* **1787**, 1352–1362 (2009).
30. Hom, J. & Sheu, S. S. Morphological dynamics of mitochondria-a special emphasis on cardiac muscle cells. *J. Mol. Cell Cardiol.* **46**, 811–820 (2009).
31. Dorn, G. W., 2nd. & Scorrano, L. Two close, too close: sarcoplasmic reticulum-mitochondrial crosstalk and cardiomyocyte fate. *Circ. Res.* **107**, 689–699 (2010).
32. García-Pérez, C., Schneider, T. G., Hajnóczky, G. & Csordás, G. Alignment of sarcoplasmic reticulum-mitochondrial junctions with mitochondrial contact points. *Am. J. Physiol. Heart Circ. Physiol.* **301**, H1907–H1915 (2011).
33. Rizzuto, R., De Stefani, D., Raffaello, A. & Mammucari, C. Mitochondria as sensors and regulators of calcium signalling. *Nat. Rev. Mol. Cell Biol.* **13**, 566–578 (2012).
34. Lu, X. *et al.* Measuring local gradients of intramitochondrial $[Ca^{2+}]$ in cardiac myocytes during sarcoplasmic reticulum Ca^{2+} release. *Circ. Res.* **112**, 424–431 (2013).
35. Cox, D. A., Conforti, L., Sperelakis, N. & Matlib, M. A. Selectivity of inhibition of Na^+-Ca^{2+} exchange of heart mitochondria by benzothiazepine CGP-37157. *J. Cardiovasc. Pharmacol.* **21**, 595–599 (1993).
36. Thu, le. T., Ahn, J. R. & Woo, S. H. Inhibition of L-type Ca^{2+} channel by mitochondrial Na^+-Ca^{2+} exchange inhibitor CGP-37157 in rat atrial myocytes. *Eur. J. Pharmacol.* **552**, 15–19 (2006).
37. Shen, J. B., Jiang, B. & Pappano, A. J. Comparison of L-type calcium channel blockade by nifedipine and/or cadmium in guinea pig ventricular myocytes. *J. Pharmacol. Exp. Ther.* **294**, 562–570 (2000).
38. Bogdanov, K. Y., Vinogradova, T. M. & Lakatta, E. G. Sinoatrial nodal cell ryanodine receptor and Na^+-Ca^{2+} exchanger: molecular partners in pacemaker regulation. *Circ. Res.* **88**, 1254–1258 (2001).
39. Palmer, A. E., Jin, C., Reed, J. C. & Tsien, R. Y. Bcl-2-mediated alterations in endoplasmic reticulum Ca^{2+} analyzed with an improved genetically encoded fluorescent sensor. *Proc. Natl. Acad. Sci. USA* **101**, 17404–17409 (2004).
40. Grandi, E. *et al.* Human atrial action potential and Ca^{2+} model: sinus rhythm and chronic atrial fibrillation. *Circ. Res.* **109**, 1055–1066 (2011).
41. Sartiani, L., Bochet, P., Cerbai, E., Mugelli, A. & Fischmeister, R. Functional expression of the hyperpolarization-activated, non-selective cation current If in immortalized HL-1 cardiomyocytes. *J. Physiol.* **545**, 81–92 (2002).
42. Deng, C. *et al.* Pharmacological effects of carvedilol on T-type calcium current in murine HL-1 cells. *Eur. J. Pharmacol.* **621**, 19–25 (2009).
43. Yang, Z. & Murray, K. T. Ionic mechanisms of pacemaker activity in spontaneously contracting atrial HL-1 cells. *J. Cardiovasc. Pharmacol.* **57**, 28–36 (2011).
44. Zhou, Z. & Lipsius, S. L. Na^+-Ca^{2+} exchange current in latent pacemaker cells isolated from cat right atrium. *J. Physiol.* **466**, 263–285 (1993).
45. Okamoto, Y., Takano, M., Ohba, T. & Ono, K. Arrhythmogenic coupling between the Na^+-Ca^{2+} exchanger and inositol 1,4,5-triphosphate receptor in rat pulmonary vein cardiomyocytes. *J. Mol. Cell Cardiol.* **52**, 988–997 (2012).
46. Himeno, Y. *et al.* Minor contribution of cytosolic Ca^{2+} transients to the pacemaker rhythm in guinea pig sinoatrial node cells. *Am. J. Physiol. Heart Circ. Physiol.* **300**, H251–H261 (2010).
47. Severi, S., Fantini, M., Charawi, L. A. & Difrancesco, D. An updated computational model of rabbit sinoatrial action potential to investigate the mechanisms of heart rate modulation. *J. Physiol.* **590**, 4483–4499 (2012).

48. Lakatta, E. G., Maltsev, V. A. & Vinogradova, T. M. A coupled SYSTEM of intracellular Ca^{2+} clocks and surface membrane voltage clocks controls the timekeeping mechanism of the heart's pacemaker. *Circ. Res.* **106**, 659–673 (2010).
49. Yaniv, Y. *et al*. Crosstalk between mitochondrial and sarcoplasmic reticulum Ca^{2+} cycling modulates cardiac pacemaker cell automaticity. *PLoS One* **7**, e37582 (2012).
50. Neco, P. *et al*. Paradoxical effect of increased diastolic Ca^{2+} release and decreased sinoatrial node activity in a mouse model of catecholaminergic polymorphic ventricular tachycardia. *Circulation* **126**, 392–401 (2012).
51. Jiang, D., Zhao, L. & Clapham, D. E. Genome-wide RNAi screen identifies Letm1 as a mitochondrial Ca^{2+}/H^{+} antiporter. *Science* **326**, 144–147 (2009).
52. Nowikovsky, K., Pozzan, T., Rizzuto, R., Scorrano, L. & Bernardi, P. Perspectives on:SGP symposium on mitochondrial physiology and medicine: the pathophysiology of LETM1. *J. Gen. Physiol.* **139**, 445–454 (2012).
53. Sanders, K. M., Koh, S. D. & Ward, S. M. Interstitial cells of cajal as pacemakers in the gastrointestinal tract. *Annu. Rev. Physiol.* **68**, 307–343 (2006).
54. Dixon, R. E. *et al*. Electrical slow waves in the mouse oviduct are dependent on extracellular and intracellular calcium sources. *Am. J. Physiol. Cell Physiol.* **301**, C1458–1469 (2011).
55. Cheong, E., Kim, C., Choi, B. J., Sun, M. & Shin, H. S. Thalamic ryanodine receptors are involved in controlling the tonic firing of thalamocortical neurons and inflammatory pain signal processing. *J. Neurosci.* **31**, 1213–1218 (2011).
56. Kadiri, L. R., Kwan, A. C., Webb, W. W. & Harris-Warrick, R. M. Dopamine-induced oscillations of the pyloric pacemaker neuron rely on release of calcium from intracellular stores. *J. Neurophysiol.* **106**, 1288–1298 (2011).
57. Brown, D. A. & O'Rourke, B. Cardiac mitochondria and arrhythmias. *Cardiovasc. Res.* **88**, 241–249 (2010).
58. Adler, J. & Parmryd, I. Quantifying colocalization by correlation: the Pearson correlation coefficient is superior to the Mander's overlap coefficient. *Cytometry A.* **77**, 733–742 (2010).
59. Patton, C., Thompson, S. & Epel, D. Some precautions in using chelators to buffer metals in biological solutions. *Cell Calcium* **35**, 427–431 (2004).
60. Bahrudin, U. *et al*. Impairment of ubiquitin-proteasome system by E334K cMyBPC modifies channel proteins, leading to electrophysiological dysfunction. *J. Mol. Biol.* **413**, 857–878 (2011).
61. Sarai, N., Matsuoka, S. & Noma, A. simBio: a Java package for the development of detailed cell models. *Prog. Biophys. Mol. Biol.* **90**, 360–377 (2006).
62. Matsuoka, S., Sarai, N., Kuratomi, S., Ono, K. & Noma, A. Role of individual ionic current systems in ventricular cells hypothesized by a model study. *Jpn. J. Physiol.* **53**, 105–123 (2003).
63. Matsuoka, S., Sarai, N., Jo, H. & Noma, A. Simulation of ATP metabolism in cardiac excitation-contraction coupling. *Prog. Biophys. Mol. Biol.* **85**, 279–299 (2004).
64. Takeuchi, A. *et al*. Ionic mechanisms of cardiac cell swelling induced by blocking Na^{+}/K^{+} pump as revealed by experiments and simulation. *J. Gen. Physiol.* **128**, 495–507 (2006).

Acknowledgements

We thank Dr. Claycomb, Dr. Tsien and Dr. Sekler for generous gifts of HL-1 cardiomyocytes, Cameleon D1ER in pcDNA3 vector and NCLX antibody, respectively. We also thank Dr. Collins for English editing. This work was supported by JSPS KAKENHI Grant Number 23689011 and 23390042 (A.T. and S.M.).

Author contributions

A.T. and S.M. designed research. A.T., B.K. and S.M. performed imaging analysis. A.T. did molecular work. A.T. and S.M. constructed a mathematical model and performed simulation analysis. A.T. and S.M. drafted the article. All authors discussed the results and approved the final version of the manuscript.

Additional information

Supplementary information accompanies this paper at http://www.nature.com/scientificreports

Competing financial interests: The authors declare no competing financial interests.

How to cite this article: Takeuchi, A., Kim, B. & Matsuoka, S. The mitochondrial Na^{+}-Ca^{2+} exchanger, NCLX, regulates automaticity of HL-1 cardiomyocytes. *Sci. Rep.* **3**, 2766; DOI:10.1038/srep02766 (2013).

This work is licensed under a Creative Commons Attribution-NonCommercial-NoDerivs 3.0 Unported license. To view a copy of this license, visit http://creativecommons.org/licenses/by-nc-nd/3.0